Available online at www.sciencedirect.com

SciVerse ScienceDirect

Journal of the European Ceramic Society 32 (2012) 2243–2251

www.elsevier.com/locate/jeurceramsoc

Characterization of vitreous enamel–steel interface by using hot stage ESEM and nano-indentation techniques

A. Zucchelli [b,*], M. Dignatici [a], M. Montorsi [a], R. Carlotti [c], C. Siligardi [a]

[a] *Department of Materials and Environmental Engineering, University of Modena and Reggio Emilia, Via Vignolese 905, 41100 Modena, Italy*
[b] *Mechanical Engineering Department, University of Bologna, Viale Risorgimento 2, 40136 Bologna, Italy*
[c] *Smaltiflex S.p.A, Via dell'Industria, 115 41038 S. Felice S/P (MO), Italy*

Received 4 July 2011; received in revised form 22 February 2012; accepted 3 March 2012
Available online 10 April 2012

Abstract

In this study, phase transformation of the vitreous enamel and the interface steel–enamel during firing was analyzed. The thermal transformation of vitreous coating on steel was observed "in situ" with an environmental scanning electron microscopy and the mechanical properties of the steel–enamel interface were studied by using a nano-indenter. The interface reactions and the resulting structure can strongly influence the adhesion mechanism between glass coatings and the metal substrate. An in-depth investigation and structural characterization was therefore performed to define the correlation between interface morphology and the final chemical and mechanical properties of the enamel–steel interface.

Keywords: Porcelain; Interfaces; Mechanical properties; Hardness; Functional applications

1. Introduction

Vitreous enamels play a very important role in the coating production process of steel in accordance with the technical and esthetic properties induced by the enamel to the final material.[1] In particular, from the functional point of view, vitreous enamel coatings show excellent resistance to chemical degradation processes[2,3] as well as a good resistance to tribological phenomena such as abrasive wear.[4] Enamel coatings are generally defined as a substantially vitreous glassy inorganic layer bonded to various metal substrates by fusion at a defined temperature. The key factor affecting the functionality of the final material is the achievement of a good bond between the enamel and the metal substrate during the enameling process. Several factors could affect interface reactions and the adhesion mechanism between the glass coatings and the metal substrate such as chemical composition of enamel, the type of steel, the roughness of the metal surface, the heating process and the temperature of glazing, the atmosphere of the oven, and so on.[5] Although many papers have been published on this topic, the base mechanism related to the metal–enamel interface formation is not still clear and needs further and in-depth investigation. The most common analytical techniques used to characterize the enamel–steel interface mainly from the chemical/mineralogical point of view include scanning electron microscopy, transmission electron microscopy, X-ray photoelectron microscopy, X-ray diffraction and dilatometric method.[6,7]

The aim of the present study is to analyze "in situ" the melting process of the enamel by using an environmental scanning electron microscope and to obtain the mechanical properties of the steel–enamel interface by using a nano-indenter. Quantitative correlation between the structure of the interface and its chemical and mechanical properties was analyzed.

Data from microstructural and chemical examination of the interface during firing were used to interpret some thermal transformations that occur "in situ", and the micromechanical test was used to correlate the diffusion of Fe-ions with the final mechanical properties of the interface.

2. Experimental procedure

2.1. Materials and sample preparation

The substrates used for enamel coating were cold rolled rectangular plates of very low carbon steel whose chemical

* Corresponding author.
E-mail address: a.zucchelli@unibo.it (A. Zucchelli).

0955-2219/$ – see front matter © 2012 Elsevier Ltd. All rights reserved.
doi:10.1016/j.jeurceramsoc.2012.03.008

Table 1
Chemical composition of enamel frit.

Oxide	SiO_2	B_2O_3	Na_2O	TiO_2	BaO	Al_2O_3	CaO	K_2O	Fe_2O_3	MnO	MgO	$(Co_3O_4 + NiO + CuO)$	Total
ICP wt.%	62.41	10.06	7.65	4.51	2.57	2.2	4.37	3.01	1.21	0.92	0.14	0.95	100

composition in wt.% is as follows: C = 0.004, Si = 0.008, S = 0.015, Mn = 0.22, P = 0.008, Al = 0.037, Ni = 0.036, Cr = 0.021, Cu = 0.032, and Fe rest. The dimensions of the sheet of steel were 30 mm × 30 mm × 0.8 mm. The first treatment of the metal sheet consisted of the elimination of grease and impurities by immersing the specimens in a chemical degreasing bath at 70 °C for 10 min. The degreasing agent was a solution of 5% (w/v) of a commercial product made of sodium hydroxide, benzenesulfonic acid and mono-C10-14 alkyl derivates produced by MAZZON. After this pre-treatment, the metal sheet was pickled in a sulfuric acid solution at 5% at 65 °C for 5 min. This removes rust and scale and increases the surface roughness that helps the subsequent treatment. To increase the oxidation of iron, the sheet metal was immersed in a bath of 1.2% (w/v) of sulfate of nickel at 68 °C. This enabled the deposition of a thin layer of nickel on the surface of the metal sheet. The addition of nickel mitigates the problems of fish-scaling and promotes adhesion between the enamel and the steel surface.[8–10] Smaltiflex S.p.A. provided the enamel studied in this work. The enamel slip was produced by milling a proper frit, whose chemical composition is reported in Table 1, with the addition in the milling chamber of 12 wt.% of SiO_2, 4 wt.% of a commercial caolinitic clay (provided by Colorobbia S.p.A.), 0.6 wt.% of $NaNO_2$, 0.6 wt.% of $NaAlO_2$ and 0.6 wt.% of H_3BO_3.

The frit was ball milled down to D90 = 45 μm and mixed with additives, clay, salts, quartz and water to form a batch of enamel slip. The enamel slip was applied to the sheet steel by a hand-spraying system. The specific gravity of enameling slip is 1.70 g/cm^3. The enameled samples were then dried in an oven at 120 °C.

The heating process, which promotes the bond creation between steel and enamel, was performed in an industrial furnace. The firing time was 6 min at 860 °C; the sample was then cooled in air. The thickness of the enamel was about 200 μm per side. This final product is named "industrial sample".

3. Sample characterization

3.1. Enamel and steel characterization

The glass transformation temperature of enamel, T_g, was determined with a Netzsch, STA 409 differential thermal analyzer (DTA) on samples milled to an average particle size of less than 25 μm. The DTA measurements were carried out on about 30 mg of sample in a Pt crucible. Data for each run were automatically collected from the DTA apparatus.

The thermal behavior and the coefficient of thermal expansion (alfa) of the enamel were measured using a hot-stage microscope using powdered enamel (<25 μm) (Model Misura, Expert System Solutions, Modena, Italy) and an optical dilatometer (Model Misura, Expert System Solutions, Modena, Italy). For the hot-stage microscope, the enamel powders were compacted to little cylinders (1 mm diameter and 3 mm of height) by uniaxial pressing. The measurements were performed with 20 °C/min heating rate from 20 °C to 1400 °C. Hot stage microscopy is a fast and simple procedure that makes it possible to approximately measure some points of the viscosity temperature curve for vitreous materials. The different stages of the process are recorded photographically or by means of a video camera. A typical series of photographs shows the evolution of the glass compact during heating. In these investigations, the shape change of the silhouette of the sample is the indicator used for assessing the physical changes occurring in the material (from sintering to melting). One of the main advantages of the heating microscope is that the specimen is at no time in contact with an external measuring element (e.g. a contact rod such as in dilatometers). Thus, no external load is applied which could alter the softening process.

In this work the viscosity–temperature curve for the studied enamel was measured by using the De Pablos method,[11] choosing four characteristic points: the transformation point ($\log \eta = 13$) (from DTA measurement), first sintering ($\log \eta = 10$), softening point ($\log \eta = 6$), half-ball ($\log \eta = 4.2$) and flow ($\log \eta = 3.0$) from hot stage microscopy. The coefficient of thermal linear expansion of the enamel was measured on a bar of 15 mm × 15 mm × 5 mm, in the 50–400 °C temperature range with a heating rate of 10 °C/min. In order to obtain the bar, the frit was melted at 1400 °C and the melt was poured into a graphite mold and cooled to room temperature. The bar was then cut in order to fit the dilatometer sample holder.

Microhardness measurements were performed on enamel and steel with a Matsuzawa DMH-2 automatic hardness tester equipped with a Vickers indenter. A total time of 15 s was used for each indentation. Each value of hardness is the average of twenty measurements with the respective standard deviation.

Measurements of surface steel roughness were performed by using DIAVITE DH-5 equipment. In order to study the thermal transformation of enamel on the steel, "in situ" environmental scanning electron microscopy (ESEM) with hot stage was used. An FEI Quanta 200 ESEM equipped with a thermal tungsten gun, a gaseous secondary electron detector (GSED), and a 1500 °C hot stage was used for in situ electron imaging. An AS-type thermocouple was used to monitor the temperature, and calibration was performed using the melting point of gold (1064 °C). The instrument was operating at 20 kV acceleration potential and with a working distance of about 10 mm. The samples were heated at a rate of about 20 °C/min. SE images were collected at several temperatures. The heating gradient and temperature interval were selected on the basis of an industrial cycle: heating rate 50 °C/min up to 900 °C. All controlled ESEM experiments were repeated twice and gave reproducible results. The sample preparation consisted of cutting a small piece of steel in a

square form (3/4 mm per side); the enamel powder was then dispersed in acetone, to create slurry. This dispersion was applied over the steel by using a laboratory air-spray. It is worth noting that the thickness of the enamel is thinner than the industrial one, since it is more or less 150 μm. This sample was named "laboratory sample".

Finally the crystalline phases formed on the enamel were monitored by an XRD diffractometer with Cu-K_α radiation and conventional θ–2θ geometry (PANAlytical, X'Pert PRO, Cu-K_α radiation equipped with an X'Celerator detector).

3.2. Enamel–steel interface characterization

To study the enamel–steel interface, a conventional high resolution scanning electron microscope (SEM) with an energy dispersion spectroscope (EDS), SEM + EDS, (Philips XL 40/604 + INCA instruments) was used. A transversal cross-section of an industrial specimen was incorporated into a resin. After the solidification, the sample was polished on the surface with silicon carbide and alumina gel papers. Finally the specimen was mounted on aluminum stub and gold-coated (10 nm thick).

The nanohardness as well as the Young modulus of the interface was determined on the polished cross-sections by depth sensing Berkovic nanoindentation (Nanoindenter, CSM Instruments, Peseux, Switzerland), using a constant size normal penetration of 200 nm. The tested sample was incorporated into resin for the measurements. This resin was thermosetting and created a sustainable system after its solidification in order to place the system on the sample port. The resin is very important in order to block the sample and prevent its movement during measurement. For the test, an indentation matrix (7 rows × 5 columns) on the steel–enamel interface was used. A semi quantitative chemical analysis by EDS was then performed on each single indentation in order to correlate the mechanical properties with the interface chemical compositions.

4. Result and discussion

4.1. Enamel and steel characterization

Fig. 1 shows the DTA thermogram of enamel: while a well-defined endothermal effect corresponding to a T_g temperature of about 480 °C was observed, no crystallization peak can be noted.

The linear thermal expansion coefficient of vitreous enamel is 12.4×10^{-6}/°C, and for steel, as reported in the literature,[12] it is 13.0×10^{-6}/°C. This small difference between the thermal expansion coefficients makes it possible to obtain the coating under compression while the steel is under tension (see Fig. 18 in[12] from which, for this specific case, it is possible to estimate a maximum residual stress acting on the coating of about −20 MPa). The introduction of surface compression is a well-established technique for strengthening of enamel because the presence of a layer of surface compression mitigates failure from coating cracks.[12,13]

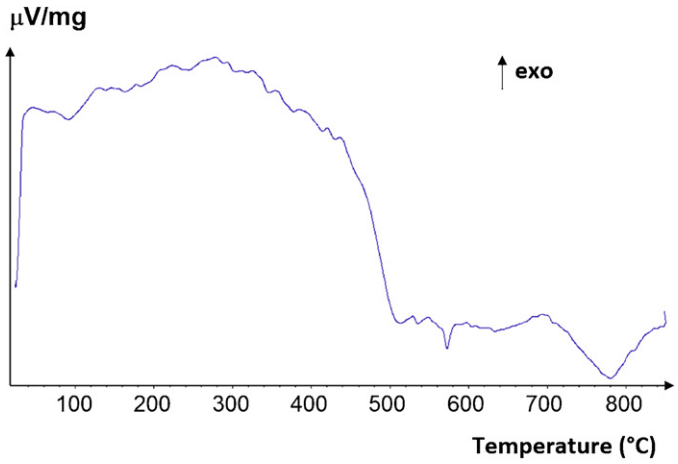

Fig. 1. DTA curve of the studied enamel.

From the hot stage microscopy experiments it was possible to observe that the sintering temperature of the enamel occurs at about 660 °C, the softening occurs at about 760 °C while the sphere is reached at about 790 °C. Finally, the hot stage microscopy experiments showed that the half-sphere of the enamel occurs at about 830 °C and the melting temperature is about 840 °C.

Fig. 2 shows a qualitative viscosity–temperature curve obtained by hot stage microscopy for the enamel samples. Since only a small temperature range was considered, the viscosity–temperature behavior is linear. It is important to underline that the atmosphere of the kiln of the hot stage microscope influences the surface tension and the wet angle, while the possible emission of gases from the enamel mainly affects the points based on the observation of definite geometrical forms such as the half ball and melting points.

In any case, this technique makes it possible to obtain a qualitative viscosity–temperature curve for the enamel in an easier way than the other more "sophisticated" techniques (beam bending, fiber elongation, high temperature rotational viscosimeter, etc...[14–16]).

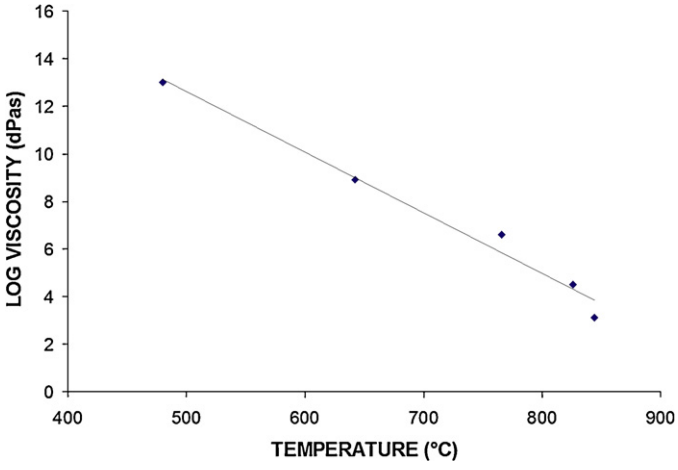

Fig. 2. Qualitative viscosity–temperature curve and the related ESEM taken during the heating of the enamel–steel system.

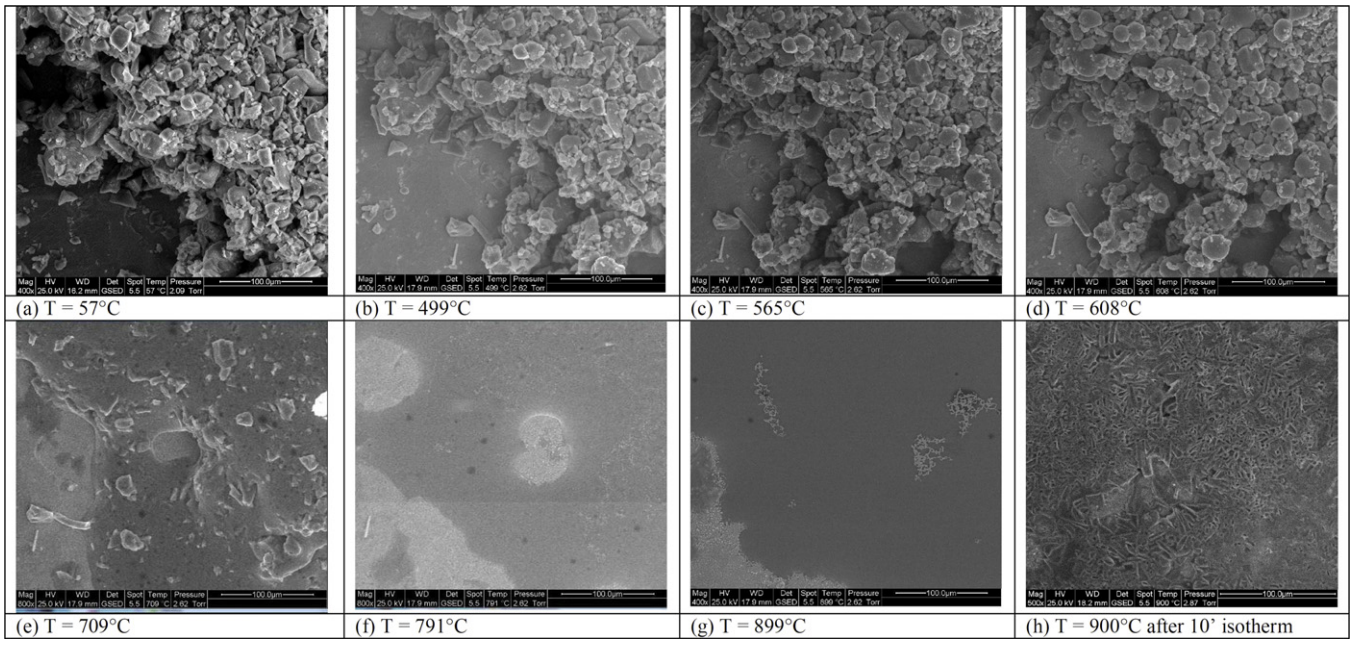

Fig. 3. ESEM "in situ" image of studied enamel during heating at different temperatures.

Surface microhardness of the enamel and of the steel are, respectively, 710 ± 20 and 129 ± 20 Vickers. Surface roughness of the enamel is: $R_a = 0.39 \pm 0.04\ \mu m$, $R_z = 2.15 \pm 0.26\ \mu m$, and $R_{max} = 2.8 \pm 0.8\ \mu m$; while the surface roughness of the steel is: $R_a = 1.07 \pm 0.19\ \mu m$, $R_z = 5.73\ \pm 0.43\ \mu m$, and $R_{max} = 7.32 \pm 0.84\ \mu m$. The measured steel roughness fits the range[9] that is known to be able to support the enamel–steel adhesion. On the other hand, the very low roughness of the enamel coating is suitable for technical applications where cleanability is mandatory. The measured microhardness can be considered as the real hardness of the enamel coating. From the functional point of view, it is relevant to note the fact that the enamel coating is 5.5 times harder than the steel base material. In fact the surface microhardness of the enamel coating plays a strategic role in technical applications where a tribological resistance is needed.

The "in situ" ESEM observation of the laboratory sample, during the enameling, provides an important tool to study the full melting process and this equipment makes it possible to record a "movie" of all the observations as well of the measurements. Fig. 3 shows in detail the morphological evolution of the enamel powder during melting, starting from room temperature up to 900 °C. Fig. 3a shows a classical crushed-glass powder; increasing the temperature above the T_g temperature the viscous flow resulting from the driving force of the surface tension causes grain rounding and neck growth (Fig. 3b–d). At about 700 °C (Fig. 4e) the enamel starts to melt even if quartz particles are clearly visible, but it becomes homogeneous and totally melted at about 900 °C. An isotherm at 900 °C for 10 min produces strong crystallization observed by XRD of Fe_2O_3 and Fe_3O_4, (Reference codes: 01-079-0007 and 00-002-1035) while the quartz is already present in the enamel as raw material (data not reported). As already reported by Barcova et al.[17] these crystalline phases are formed during heating because an intensive thermal effect induces an oxidation process on the enamel surface, which takes place according to the following pathway: $\alpha\text{-Fe} \rightarrow Fe_3O_4 \rightarrow \alpha\text{-}Fe_2O_3$. The oxygen supply is very important during the thermal process because we obtain different chemical reactions at different temperatures. Water can be a good supply of oxygen to obtain the oxidation of the iron.[6]

$$\mathrm{NiO(precoat)} + \mathrm{Fe(steel)} \rightarrow \mathrm{FeO(oxidelayer)} + \mathrm{Ni(oxidelayer)}$$

$$\mathrm{d}G^{\circ}(\mathrm{J/molFeorC}) = \mathrm{dH}^{\circ} - \mathrm{Td}S^{\circ} \quad \mathrm{d}G^{\circ}(\mathrm{J/molFeorC}) = -28,137 - 21.8\,\mathrm{T}$$

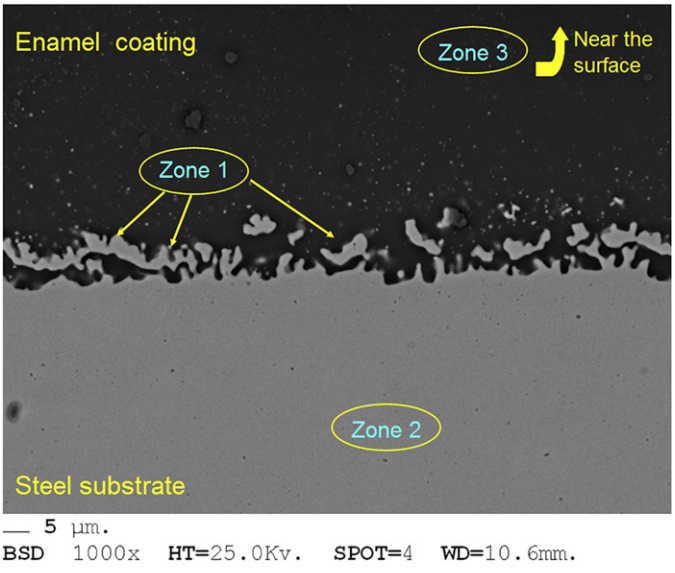

Fig. 4. SEM micrograph of cross sectioned enamel/steel interface.

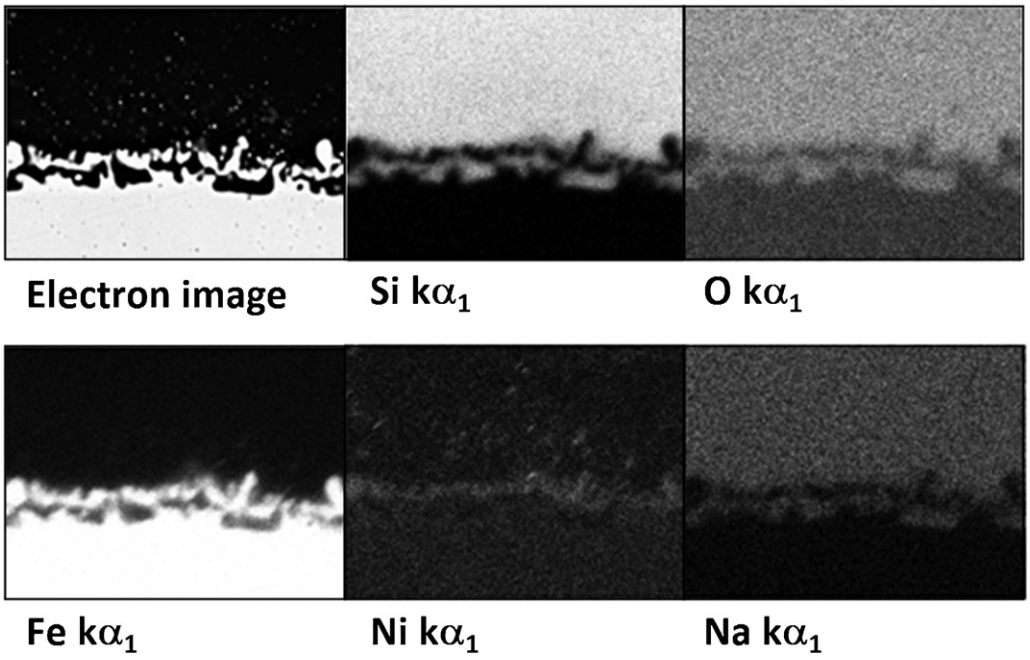

Fig. 5. X-ray mapping of interface.

$$\mathrm{Fe(steel)} + \mathrm{H_2O(steam)} \rightarrow \mathrm{H_2(gas)} + \mathrm{FeO(oxidelayer)}$$

$$\mathrm{d}G^{\circ}(\mathrm{J/molFeorC}) = \mathrm{d}H^{\circ} - T\mathrm{d}S^{\circ} \quad \mathrm{d}G^{\circ}(\mathrm{J/molFeorC}) = -16,245 + 8.6\,T$$

$$2\mathrm{Fe(steel)} + 3\mathrm{H_2O(steam)} \rightarrow \mathrm{Fe_2O_3(oxidelayer)} + 3\mathrm{H_2(gas)}$$

$$\mathrm{d}G^{\circ}(\mathrm{J/molFeorC}) = \mathrm{d}H^{\circ} - T\mathrm{d}S^{\circ} \quad \mathrm{d}G^{\circ}(\mathrm{J/molFeorC}) = -35,861 + 41.6\,T$$

In fact, ferric and ferrous cations play different roles in the structure of melt, so the ferric–ferrous ratio influences the physical properties of melts. The redox state of iron in melts depends on some external and internal parameters: temperature, oxygen fugacity and composition. The authors would like to underline that the oxygen concentration in the sample was measured in an industrial sample, after heat treatment in SEM equipment not in situ in ESEM equipment. ESEM was used only to understand how the enamel melts on steel during the heat treatment.

4.2. Steel–enamel interface characterization (industrial sample)

A typical micrograph of the enamel–steel interface using back scattered electrons for imaging is shown in Fig. 4. This figure shows small islands in the interfacial region, Zone 1. It can be noted that the islands form the so-called anchor points; thus the roughness of steel in the interface is increased.[18]

Several EDS spectra, twenty, were collected in three different zones of enamel, Fig. 5: near metal; above "islands" and near the surface; the average semi quantitative chemical analysis of the main oxides is reported in Table 2.

Analysing the same zone by using X-ray mapping, Fig. 5 shows a distribution of Si, O, Na, Fe and Ni elements in the interface. While anchor points are mainly composed of Fe and Ni (observed by EDS but the spectrum is not reported), enamel can be found around these "small islands", as confirmed by the presence of Si, O and Na. Observing the Ni-map, it was found that the interface is mainly composed of Ni and Fe even if very small Ni-richer areas are clearly evident in the enamel phase.

The equipment used to detect the amount of element on the studied samples is an energy dispersive spectroscope (INCA instruments). The microanalysis software has a built-in routine to transform the element % concentration in weight oxide %. As reported in[27] the X-ray intensity generated for each element in the sample is proportional to the concentration of that element. The quantitative analysis used in this work is a "standardless analysis". Standardless analysis is the simplest of the correction procedure. The spectrum of the unknown is recorded without concern for the electron dose as long as the dead time is acceptable. To perform a quantitative analysis, it is necessary only to supply the correct beam energy and the elements to be analyzed. The analysis total will always be exactly 100%. This

Table 2
semiquantitative chemical analysis of the three different zones of the enamel (see Fig. 4).

Zones	Oxide wt.% (±1%)			
	Na_2O	SiO_2	Fe_2O_3	Others
Zone 1	6.9	38.6	45.4	9.1
Zone 2	7.8	57.5	22.4	12.3
Zone 3	9.0	71.0	1.8	18.2

approach is that we can calculate the intensity measured from standards with accuracy equal to that measuring them directly, based on certain properties of the single spectrum obtained from an unknown. The most general approach makes use of four equations to predict the X-ray intensity that would be obtained from a pure-element standard.[27]

From the results it is clear that the concentration of iron oxides at the top of the enamel layer is 1 wt.%, while the presence of higher Fe concentrations at the interfacial enamel must be caused by a reaction between enamel and steel as well as the dissolution of any iron oxide phases formed during firing.

As reported by Dumm and Brown,[19] iron concentration was measured mainly as Fe^{2+}, since Fe^{3+} is not stable at 850 °C in the presence of iron.

At the interface we had the presence of FeO and islands rich in FeNi at the intergrowth phase. The equilibrium at the interface, in the pretreatment, is shown by this reaction:[6]

$$\text{NiOprecoat} + \text{Festeel} \rightarrow \text{FeOoxidelayer} + \text{Ni oxidelayer}$$

$$dG^{\circ}(\text{J/molFeorC}) = dH^{\circ} - \text{Td}S^{\circ} \quad dG^{\circ}(\text{J/molFeorC}) = -28,137 - 21.8\,\text{T}$$

As reported by Sorensen et al.,[20] the Fe^{2+} ions behave as network modifiers, while the Fe^{3+} ions preferably behave as network formers; this means that the viscosity of enamel in the interface should have a lower viscosity with respect to industrial enamel during firing, especially at higher temperatures, increasing the diffusion of iron from the steel. For the same reason, the coefficient of linear expansion of enamel in the interface having higher amounts of network modifier will present a CTE value lower than the steel one (13.0×10^{-6}/°C). This fact can contribute to increase the compressive stress in the enamel layer at the interface region.

At the same time, it is important to underline that, as reported by Romero and Rincon,[21] thanks to TEM observation of glasses with similar composition, iron oxide in the glass seems to promote a liquid–liquid phase separation in the original enamel where drops richer in iron are dispersed in the silica-vitreous phase. The industrial sample was also subjected to a fractographic analysis after an impact test as described in.[12] From the SEM observation of the fractured surface, a morphology close to a known liquid–liquid phase separation was observed.[22] The liquid formed during melting of a glass batch can, in some cases, spontaneously separate into very viscous liquids or phases. Cooling the melts to a temperature below the glass transformation leads to a phase separation as a result of a liquid–liquid immiscibility. Understanding of immiscibility is based on thermodynamics of regular solutions. The separation process can yield glass with either droplet/matrix or interconnected microstructures.[26] In particular, in glasses containing high amounts of iron, the EDS analysis indicates the presence of two phases rich in iron oxide (mainly crystalline) and silicon oxide (mainly vitreous), respectively.

This phase separation can act as a nuclear agent for the crystallization of iron rich phases.

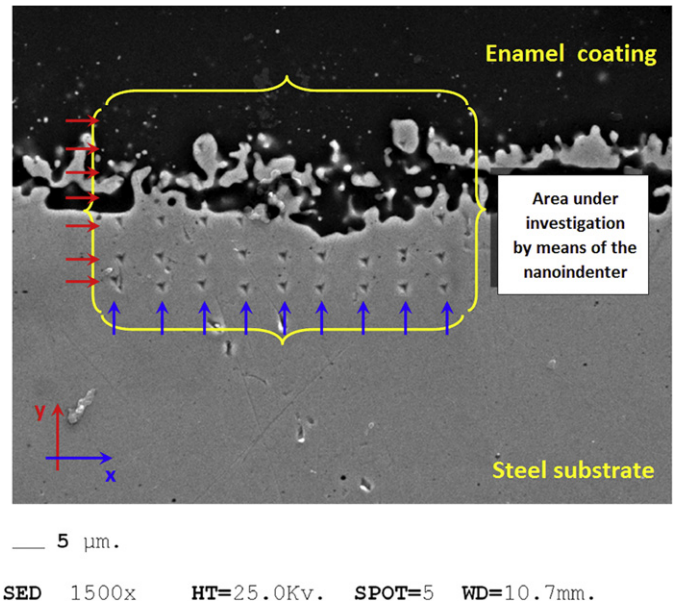

Fig. 6. SEM indentation matrix zone on enamel–steel interface at 1500× of magnification.

Since the steel–enamel interface presents a very complex chemical composition due to the diffusion of Fe ions, the microhardness of this zone will show different mechanical properties with respect to the other enamel and the steel constituents. As reported above, the thickness of the interface is in the range of 35–40 μm and it is quite difficult to measure its mechanical properties by Vickers microhardness because the indentation area is usually larger than 20 μm. For these reasons, a nanoindentation technique is used to map cross-section hardness from the enamel–steel junction to the outer enamel surface. Fig. 6 shows a cross-section of the industrial sample tested by using a nano-indenter; in particular, the indentation matrix area is formed by 9 columns in *x* direction and 7 rows in *y* direction.

Fig. 7 reports Vickers Hardness with matrix points of single indentation. The distance between each horizontal and vertical line of the matrix is 5 μm, so they are equidistant in the *xy* plane.

The variability in this plot is largely due to the variation of concentration of metal oxides in the enamel interface. As an example, in Fig. 8B, we report the iron (Fe) and the silicon (Si) atomic concentration diagrams respect the position in the interface. A more evident diagram of the hardness variation can be obtained by a mean value of the hardness along each line with respect to the material constitution. Such a diagram is shown in Fig. 8C, where the mean values and the standard deviation of the HV hardness obtained by means of nanoindentation are related to the measurement positions through the specimen thickness.

The increase of hardness from the steel to enamel is due to the fact that the interface-enamel has a higher amount of Fe^{2+} than the surface-enamel and, as already reported, it acts as a network modifier; this means that some properties, such as hardness, chemical, thermal and so on, decrease with the increase of iron content in the glass.[23–25] As reported by Romero and Rincon,[21] glasses containing higher amounts of iron oxide (15–25 wt.%) give Vickers hardness values in the 571–685 HV

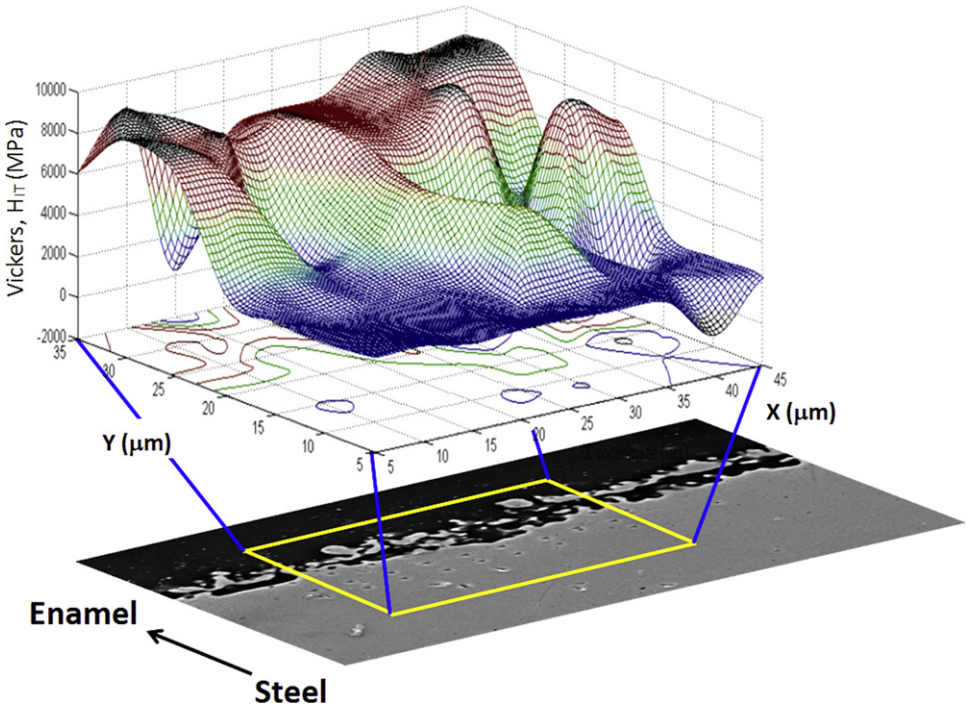

Fig. 7. Vickers map by interpolation of nanoindentations values: enamel – red; steel – blue; yellow/light blue – interface. (For interpretation of the references to color in this figure legend, the reader is referred to the web version of the article.)

range in agreement with the values of Vickers hardness obtained for the enamel-interface. On the contrary, the Young modulus, see Fig. 8D, showed a decreasing trend from the steel to the enamel layer. Such behavior can be explained by the fact that the Young modulus of silicate glasses is usually 70 GPa while for the low-carbon steel it is close to 150 GPa; increasing the glassy phase content in the interface thus decreases the Young modulus.

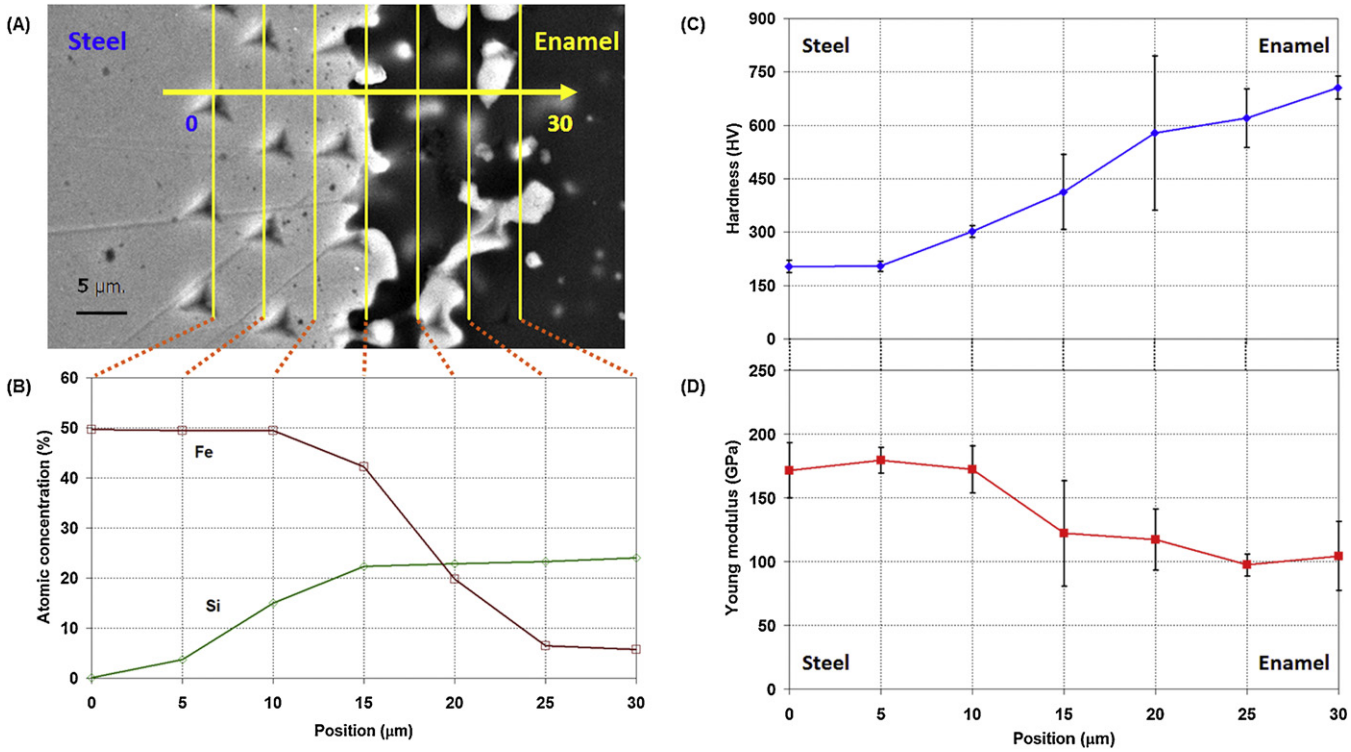

Fig. 8. (A) detail of the indented area; (B) iron (Fe) and silicon (Si) percentage concentration versus position in the interface area; (C) hardness and (D) Young modulus trends versus position in the interface area.

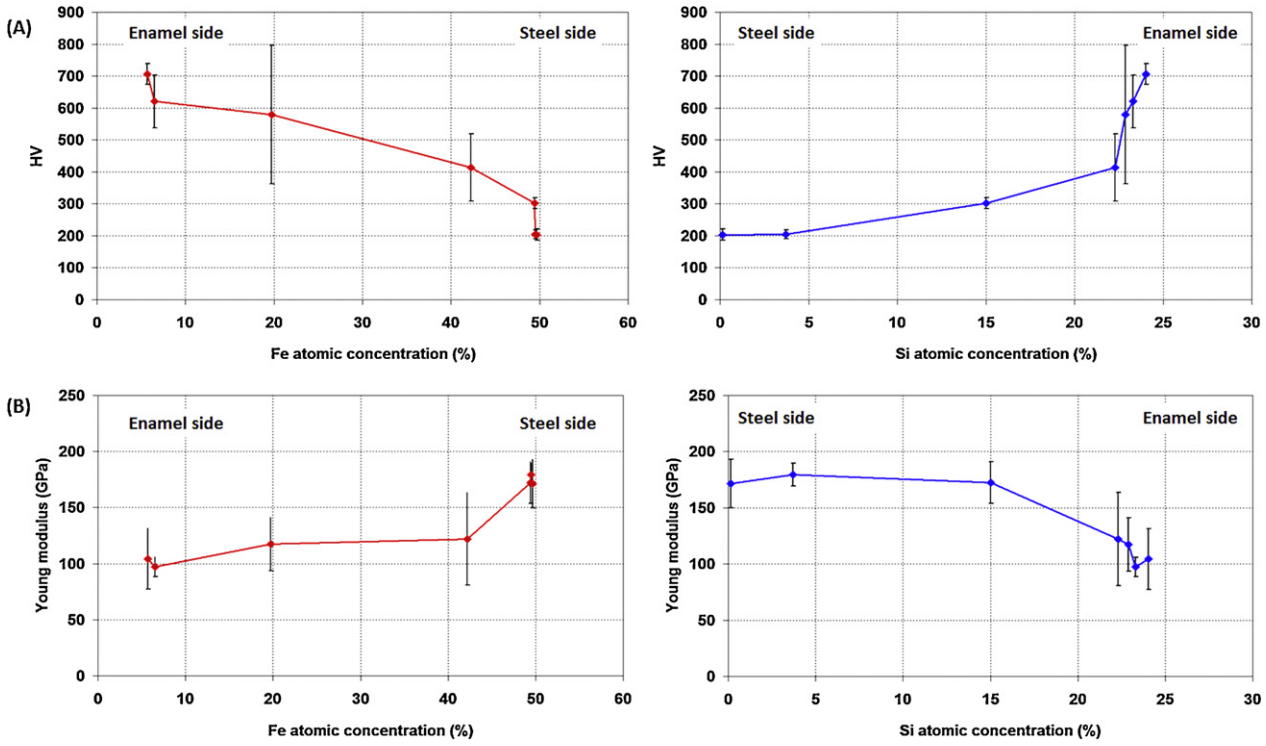

Fig. 9. (A) HV and (B) Young modulus trends with respect to the iron and silicon percentage content.

In Fig. 9A HV versus iron and silicon percentage concentrations are reported and the data show that microhardness increased from the steel to the enamel. Fig. 9A clearly shows a significant gradient in the interface nanoindentation hardness going from the outer to the interior enamel (part in contact with the steel). The outer enamel exhibits the highest hardness and was consistent with the fact that the enamel contains higher amounts of silicon, which is a former network ion. The hardness in the interior enamel decreased significantly, and this reduction is due to the fact that the enamel contains high amounts of iron ion which is, as reported above, a network modifier ion. Fig. 9B shows the Young modulus versus the iron and the silicon percentage content. On the contrary, with respect to what is observed in the case of the material hardness, the Young modulus decreases as the silicon percentage content increases and as the iron percentage content decreases. As it was observed by Sorensen et al.,[20] the concentration of iron has a significant influence on the crystallization behavior of the glass, and due to the fact that the enameling is a high temperature process in an oxidizing environment, the iron, that diffuses from the steel plate, could promote the formation of stable crystalline phases[20] into the enamel coating so locally enhancing the mechanical performances and in particular the Young modulus as highlighted by the experimental results.

From a general point of view, it can be observed that the interface between the steel and the enamel is formed by a graded interface material, where due to a gradual variation of the elements from the steel to the enamel it is possible to obtain a gradual variation in the main material properties such as hardness and elasticity.

5. Conclusions

The study reported in the present paper aims to increase the understanding of the characteristics and properties of the enamel–steel interface. Due to the fact that the enamel–steel interface is one of the most strategic and at the same time critical aspects that influence the quality and the behavior of the enamel coating, its understanding is crucial. With respect to previous papers reporting studies on the enamel–steel interface, in this study the authors used recent techniques, such as nanoindentation, and some consolidated techniques, such as hot stage ESEM analysis, in a nonconventional way in order to investigate the chemistry and the mechanical properties of the interface. The present study provided confirmation of the complex diffusion processes of material constituents that take place during enamel–steel system maturing at high temperature; it was discovered that such a diffusion process enabled the formation of some phase separations that can act as a nuclear agent for the crystallization of iron rich phases. These iron rich phases influence the adherence of the enamel as well as the hardness and the elasticity of the interface. By means of the nanoindentation techniques, the interface hardness and the Young modulus were analyzed and a trend of increasing hardness from the steel side to the enamel one was observed. On the contrary, the elasticity of the interface decreased from the steel side to the enamel one. Such behavior is very well supported by the diagrams that relate the iron and the silicon values to the hardness and the Young modulus. These diagrams confirm the influence of the chemical composition on the enamel–steel interface mechanical properties.

Acknowledgments

Thanks are due to Smaltiflex SpA for their financial support as well as a special thanks to the Emilia Romagna Region that provided the general contract research sponsorship. Many thanks to Ing. Giovanni Bolelli for performing the nanoindentation measurements. Dott. Massimo Tonelli of the Centro Interdipartimentale Grandi Strumenti, University of Modena and Reggio Emilia is kindly acknowledged for his help and support.

References

1. Andrew AI. *Porcelain enamels*. Champaign, IL: Garrad Press; 1961.
2. Kuchinski FA. Corrosion resistant thick films by enamelling. In: Wachtman JB, Haber Ra, editors. *Ceramic films and coatings*. Park Ridge, NJ: Noyes Publications; 1993. pp. 77–130.
3. Scrinzi E, Rossi S. The aesthetic and functional properties of enamel coatings on steel. *Materials and Design* 2010;**31**:4138–46.
4. Bazayants GV, Svetlichnyi VA, Demchuk VV, Ryzhikov VA. Abrasive wear of glass enamels and slag sitall used in heat energetics. *Glass and Ceramics* 1983;**40**(16):295–6.
5. Ubertazzi A, Wojciechwski N. *Vitreous enamel*. Milan: Hoepli Editor; 2002.
6. Yang X, Jha A, Brydson R, Cochrane RC. An analysis of the microstructure and interfacial chemistry of steel–enamel interface. *Thin Solid Films* 2003;**443**:33–45.
7. Peterson M, Michael Bernardin A, Cabral Kuhnen N, Gracher Riella H. Evaluation of the steger method in the determination of ceramic-glaze joining. *Materials Science Engineering A* 2007;**466**:183–7.
8. Kautz K. The effect of iron surface preparation upon enamel adherence. *Journal of the American Ceramic Society* 1937;**20**:288–95.
9. Richmond JC, Moore DG, Kirkpatrick HB, Harrison WN. Relation between roughness of interface and adherence of porcelain enamel to steel. *Journal of American Ceramic Society* 1953;**36**(12):410–6.
10. Salamah MA, White D. Catalytic activity of nickel at the glass/metal interface in the porcelain enameling system. *Journal of American Ceramic Society* 1981;**64**(4):224–6.
11. De Pablos A, Duran A, Nieto MI. Adjusting of laboratory filature furnace for obtaining fibreglass. *Boletin de la Sociedad Espanola de Ceramica Y Vidrio* 1997;**36**(5):517–23.
12. Zucchelli A, Minak G, Ghelli D. Low-velocity impact behaviour of vitreous enamelled steel plates. *International Journal of Impact Engineering* 2010;**37**:673–84.
13. Tandon R, Green DJ. Residual stress determination using strain gage measurements. *Journal of the American Ceramic Society* 1990;**73**(9): 2628–33.
14. DeHoffa PH, Anusaviceb KJ. Creep functions of dental ceramics measured in a beam-bending viscometer. *Dental Materials* 2004;**20**: 297–304.
15. Barbieri L, Leonelli C, Manfredini T, Siligardi C. Influence of viscosity on the crystallization of some anorthite-diopside glass precursors. *Journal of Materials Science Letters* 1993;**12**:294–6.
16. Siligardi C, Lusvarghi L, Montorsi M, Vernia M. Sintering and crystallization of $CaO–Al_2O_3–ZrO_2–SiO_2$ glasses containing different amount of Al_2O_3. *Journal of American Ceramic Society* 2008;**91**(3):990–5.
17. Barcova K, Mashlan M, Zboril R, Filip J, Podjuklova J, Hrabovska K, Schaaf P. Phase composition of steel–enamel interfaces: effects of chemical pretreatment. *Surface & Coating* 2006;**210**:1836–44.
18. Shieu FS, Lin KC, Wong JC. Microstructure and adherence of porcelain enamel to low carbon steel. *Ceramics International* 1999;**25**:27–34.
19. Dumm JQ, Brown PW. Dissolution of iron in silicate melts. *Journal of the American Ceramic Society* 1999;**82**:987–93.
20. Sorensen PM, Pind M, Yue YZ, Rawlings RD, Boccaccini AR, Nielsen ER. Effect of the redox state and concentration of iron on the crystallization behaviour of iron-rich aluminosilicate glasses. *Journal of Non-Crystalline Solids* 2005;**351**:1246–53.
21. Romero M, Rincon JMa. Preparation and properties of high iron oxide content glasses obtained from industrial wastes. *Journal of the European Ceramic Society* 1998;**18**:153–60.
22. Varshneya AK. *Fundamentals of inorganic glasses*. Academic Press, Inc; 1994. pp. 61–86.
23. Piscella P, Pelino M. Thermal expansion investigation of iron rich glass-ceramic. *Journal of the European Ceramic Society* 2008;**28**:3021–6.
24. Barbieri L, Corradi A, Lancellotti I. Thermal and chemical behaviour of different glasses containing fly ash and their transformation into glass–ceramics. *Journal of the European Ceramic Society* 2002;**22**:1759–65.
25. Karamanov A, Pelino M. Crystallization phenomena in iron-rich glasses. *Journal of Non-Crystalline Solids* 2001;**281**:139–51.
26. Shelby JE. *Introduction to glass science and technology*, 29, 2nd ed. Cambridge, UK: Royal Society of Chemistry; 2005. pp. 48–68.
27. Goldstein JI, Newbury DE, Echlin P, Joy DC, Romig jr AD, Lyman CE, Fiori C, Lifshin E. *Scanning electron microscopy and X-ray microanalysis*. 2nd ed. New York: Plenum Press; 1994. pp. 417–547.